Heavy Quarkonia sector in PYTHIA 6.324: tuning, validation and perspectives at LHC(b)

Public Note

Issue: 1
Revision: 0

Reference: LHCb-2007-042
Created: January 17,2007
Last modified: June 25, 2007

Prepared by: M. Bargiotti[1], V. Vagnoni[2]
[1]*CERN, Geneva, Switzerland*
[2]*INFN, Sezione di Bologna, Italy*

Abstract

In this note we investigate the impact of the recent insertion of Color Octet Model processes in PYTHIA version 6.324, through a tuning of different PYTHIA parameters, including the low-p_T behaviour. The Non-relativistic QCD parameters have been chosen according to the most recent theoretical calculations and fits to CDF data. This analysis has been mainly focused on J/ψ and Υ prompt production, with a comparison of the Monte Carlo predictions with available data from CDF at Run I and Run II energies. A prediction at the LHC energy, within different acceptance regions (CMS-Atlas and LHCb ones), is also given.

Contents

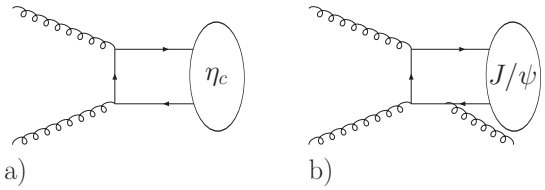

Figure 1 Leading order diagrams in CSM for the production of η_c (a) and J/ψ (b). In the CSM, the leading order J/ψ production is $O(\alpha^3)$ as a consequence of C-parity conservation.

1 Introduction

The LHCb experiment will start operating at LHC by 2007, with the aim of performing precise measurements of CP-violation arising in the beauty-quark flavor sector.

Prompt J/ψ signals are important for LHCb physics, as they can be potential backgrounds (in combination with other particles) for B$\rightarrow J/\psi\ X$ decays, and can in addition be used for calibrating the proper time resolution. Similar considerations hold for the general purpose detectors Atlas and CMS, which include in their physics programmes B physics as well, and are moreover interested in establishing the thresholds for the muon trigger lines. The possibility of evaluating the impact of the inclusion of several heavy quarkonium theories - e.g. the Color Singlet Model (CSM), Non-Relativistic QCD (NRQCD), the Color Evaporation Model (CEM) - directly on a general purpose Monte Carlo (MC) like PYTHIA [1] could be of great interest not only for the LHCb community, but for all the LHC experiments. In fact, starting from PYTHIA 6.324, NRQCD processes have been introduced in the PYTHIA code, and some room in the common blocks has been reserved for NRQCD matrix elements. The aim is to allow for a possibly better agreement between MC and real data. In Sec. 2 the motivations for the inclusion of NRQCD contributions in PYTHIA will be discussed, and a description of NRQCD milestones will be given in Sec. 3. In Sec. 4 we examine how the new matrix elements have been inserted in the PYTHIA framework. In Sec. 5 we will cover the tuning and show the results obtained with our approach, and compare them to real data. In Sec. 6 we will present the results that we obtain at the LHC energy and relevant acceptance regions.

2 Motivations for the inclusion of NRQCD in PYTHIA

The status of production of charm and beauty hidden flavor states in PYTHIA was incomplete. In fact, until PYTHIA version 6.323, only color singlet processes were implemented.

In the CSM it is assumed that a $c\bar{c}$ pair is created in a color neutral state with the same quantum numbers as the charmonium state. The same holds for the production of a $b\bar{b}$ pair. The first implication is that only a subset of diagrams for the $c\bar{c}$ production can contribute to the final state: no charmonium state can be produced from a s-channel gluon because of color neutrality. Moreover, because of C-parity conservation, the creation of a J/ψ from gluon fusion at leading order is forbidden. Therefore, the lowest order diagrams are $\mathcal{O}(\alpha_S^3)$ for the production of the J/ψ, and $\mathcal{O}(\alpha_S^2)$ for the production of the η_c (see Fig. 1).

The probability that a $c\bar{c}$ pair with correct quantum numbers will bind into a charmonium state H is given by the square of the radial wave-function at the origin:

$$\sigma(H(^{2S+1}L_J)) = \mid \frac{d^l}{dr^l} R_{nl}(0) \mid^2 \sigma(c\bar{c}(^{2S+1}L_J)). \tag{1}$$

The wave-function R_{nl} can be calculated from the Schrödinger equation with a potential V(r) given by:

$$V(r) = -\frac{4}{3}\frac{\alpha_S(1/r^2)}{r} + K^2 r \tag{2}$$

Its value at the origin can be obtained from the leptonic decay width [2], i.e.:

$$\Gamma(\psi(nS) \to l^+l^-) = \frac{16\alpha^2}{9M^2_{\psi(nS)}} \mid R_{nS}(0) \mid^2 [1 - \frac{16}{3}\frac{\alpha_S(m_c^2)}{\pi}]. \quad (3)$$

The CSM prediction for the ratio of direct J/ψ and ψ' productions:

$$\frac{\sigma^{\psi'}}{\sigma^{J/\psi}} = \frac{\Gamma(\psi' \to l^+l^-)M^3_{J/\psi}}{\Gamma(J/\psi \to l^+l^-)M^3_{\psi'}} \approx 0.24, \quad (4)$$

is in good agreement with the measured value of 0.23 [3]. However, the prediction that $\sigma^{J/\psi}$ should be one order in $\alpha_S(m_c^2) \approx 0.20$ smaller than σ^{χ_c}, is in disagreement with observation at fixed target energies, where similar rates are observed. Moreover, the CSM fails to describe the data for J/ψ and ψ' production at high p_T. Such high p_T J/ψ production is dominated by gluon fragmentation that, in CSM, can occur only in associations with two hard gluons, and is therefore suppressed by α_S^2.

Furthermore, on the practical point of view of MC generators, the previous versions of PYTHIA could not allow for a simultaneous production of J/ψ and Υ(1S), nor Υ(1S) and Υ(2S), etc.. Following the discussion started at a LCG/GENSER meeting in March 2005, T. Sjostrand introduced the NRQCD matrix elements for heavy quarkonia production in PYTHIA 6.324.

3 Brief overview of NRQCD theory

A significant step forward in the studies of heavy quarkonium phenomenology has been taken by Bodwin, Braaten and Lepage [4], who provided a new framework for the study of heavy quarkonium production and decay within QCD. In this new formalism, perturbative factorization is obtained by allowing the hevay quarkonium production and decay to take place via intermediate $Q\bar{Q}$ states with different quantum numbers than those of the physical state, that is produced or decaying.

In this new kind of approach, one of the cornerstones is based on the fact that heavy quarkonia bound states are inherentely non-relativistic. The physics of heavy quarkonia involves consequently several energy scales which are separated by the small velocity v of the heavy constituents inside the $Q\bar{Q}$ bound states. The most important scales are set by the mass M_Q, momentum $M_Q v$ and kinetic energy $M_Q v^2$ of the heavy quark and antiquark.

In order to keep track of this scale hierarchy, an effective field theory, NRQCD, has been established. This effective field theory is based upon a double power series expansion in the strong interaction fine structure constant $\alpha_S = g_S^2/4\pi$ and the velocity parameter $v \sim 1/logM_Q$. Heavy quarkonia are described within the NRQCD framework in terms of Fock state decompositions. The wave-function of a S-wave ortho-quarkonium vector meson looks schematically like:

$$\begin{aligned} |\psi_Q\rangle \quad = \quad & O(1)|Q\bar{Q}[^3S_1^{(1)}]\rangle + O(v)|Q\bar{Q}[^3P_J^{(8)}]g\rangle \\ & + O(v^2)|Q\bar{Q}[^1S_0^{(8)}]g\rangle + O(v^2)|Q\bar{Q}[^3S_1^{(1,8)}]gg\rangle \\ & + O(v^2)|Q\bar{Q}[^3D_J^{(1,8)}]gg\rangle + ... \end{aligned} \quad (5)$$

The spin, orbital and total angular momentum quantum numbers of the $Q\bar{Q}$ pairs in each Fock component are indicated in square brackets in spectroscopic notation, while the color assignment is specified by singlet or octet superscripts.

If the relative importance of various production channels depended solely upon the order in v at which pairs hadronize into physical bound states, those modes which proceed through the leading Fock component in quarkonia wave-functions would generally be dominant. This is the basic assumption of the previously quoted CSM, where heavy quarkonium production is presumed to be mediated by parton reactions that generate colorless heavy quark-antiquark pairs with the same quantum numbers as the mesons into which they non-perturbatively evolve.

The breakdown of this kind of approach steams from its neglect of all high energy processes that create $Q\bar{Q}$ pairs with quantum numbers different from those of all final state mesons.

In the formalism of NRQCD, the general expression for a production cross-section of a heavy quarkonium state H can be written as:

$$d\sigma(H+X) = \sum_{\mathcal{Q}} d\hat{\sigma}(Q\bar{Q}[\mathcal{Q}] + X')\langle\mathcal{O}^{\mathcal{H}}(\mathcal{Q})\rangle. \quad (6)$$

Here $d\hat{\sigma}(Q\bar{Q}[\mathcal{Q}] + X')$ describes the short-distance production of a $Q\bar{Q}$ pair in the color, spin and angular momentum state $\mathcal{Q} \equiv^{(2S+1)} L_J^{[1,8]}$, and $\langle\mathcal{O}^{\mathcal{H}}(\mathcal{Q})\rangle$, the vacuum expectation value of a four-fermion operator defined within NRQCD [5, 6], describes the hadronization of the pair into the observable quarkonium state H. $Q\bar{Q}$ states with quantum numbers other than H arise from the expansion of the H Fock-state wave-function in powers of the heavy-quark velocity v.

The relative importance of the different contributions in Eq. (6) can be estimated using NRQCD velocity scaling rules [6], which allow for the truncation of the series at any order of accuracy. If only the lowest order in v is retained, the description of S-wave quarkonia production or annihilation reduces to the CSM one. In the case of P-waves, instead, contributions from color-octet S-wave states are at the same order in v, as those from the leading color-singlet P-wave states.

Infrared singularities, which appear in some of the short-distance coefficients of P-wave states, can then be shown [4] to be absorbed into the long-distance part of color-octet S-wave terms, thereby ensuring a well defined overall result. A striking consequence of the NRQCD approach is that the effect of color-octet contributions can be extremely important even in the case of S-wave decay or production. In fact, while their effects are predicted to be suppressed by powers of v with respect to the leading color-singlet ones, their short-distance coefficients can be enhanced by the details of the hard interaction. There are several examples of the employment of this mechanism: for instance, the first and most important phenomenological success of this approach is the inclusion of these color-octet processes to obtain a more satisfactory description of the Tevatron data [8, 9, 10], in conjunction with the observation that gluon fragmentation provides the dominant contribution to the short-distance coefficients at large p_T [7].

The cornerstone of the predictive power of NRQCD is the so called "universality" of the non-perturbative matrix elements, i.e. the fact that their values do not depend on the details of the hard process, and so parameters extracted from a given experiment can be exploited in different ones. Several studies of experimental data coming from different kinds of reactions have been performed to assess the validity of universality. For example, calculations of inclusive quarkonia production at fixed target experiments [11], in e^+e^- [13], γp [14] collisions and B decays [15] have been carried out within this framework. Some of the most interesting predictions of the factorization approach have not been confirmed experimentally, and in some cases the overall agreement between theory and data cannot be considered satisfactory, clear indication that large uncertainties are still present. It is therefore important to assess to what extent universality is applicable.

Several potential sources of universality violation are indeed present, both at perturbative and non-perturbative level. In fact, there are potentially large corrections to the factorization theorem itself. In the case of charmonium production, for example, the mass of the heavy quark is small enough for non-universal power-suppressed corrections to be large. Furthermore, some higher order corrections in the velocity expansion are strongly enhanced at the edge of phase space [16]. In fixed target experiments, it was found that inclusion of color-octet production channels removes large discrepancies between experiment and the predictions of CSM for the total production cross-section. The inclusion of octet contributions accounts for the observed direct to total J/ψ production ratio.

A fit to fixed target data requires smaller color octet matrix elements than those extracted from high-p_T production at the Tevatron. It was argued [11] that this difference can be explained by systematic differences in the velocity expansion for collider and fixed-target predictions. In this way, while the color-octet mechanism appears to be an essential part of a satisfactory description of fixed target data, important discrepancies remain for the χ_{c1}/χ_{c2} production ratio and the J/ψ (ψ') polarization.

4 NRQCD in PYTHIA

The PYTHIA implementation for NRQCD already existed since a few years, but it was never validated nor included in any official release. The original code for the inclusion of NRQCD matrix elements in

PYTHIA has been developed by Stefan Wolf [17]. The integration of the code into PYTHIA, starting from version 6.324, has been done by T. Sjostrand in August 2005. The code has been tested and validated through this analysis, using realistic NRQCD parameters. This new release of PYTHIA is now able to refer both to charmonia and bottomonia sectors; moreover there is the possibility to produce simultaneously J/ψ with χ_c and Υ with χ_b, introduced as different processes. Some more processes, like the simultaneous production of ψ' and Υ(2S), not yet implemented, can be easily added in a future version. Originally only the contributions from CSM to the quarkonia production were implemented, until PYTHIA 6.323. NRQCD predicts nevertheless large contributions via the color octet mechanism. Therefore some new sub-processes have been introduced, for S- and P-waves, both for charmonia and bottomonia.

In this way, for sake of completeness, some processes already present in the color singlet framework have been repeated in the current formalization, only differing by wave function and matrix elements normalization factors:

$$\langle \mathcal{O}^{J/\psi}[^3S_1^{(1)}]\rangle = \frac{3N_c}{2\pi}|R(0)|^2 \quad (7)$$

$$\langle \mathcal{O}^{\chi_{c0}}[^3P_0^{(1)}]\rangle = \frac{3N_c}{2\pi}|R'(0)|^2 \quad (8)$$

Analogously to the CSM, NRQCD parametrizes the non-perturbative fragmentation of the $Q\overline{Q}$ pair into the quarkonium state. However, the extension to the Color Octet Model (COM) demands additional parameters. In fact, while CSM needs only 2 parameters, the wave-function at the origin squared $|R(0)|^2$ and its derivative $|R'(0)|^2$, NRQCD needs 10 matrix elements $\langle \mathcal{O}^H[^{2S+1}L_J^{(C)}]\rangle$ to denote the probability that a $Q\overline{Q}$ pair in a state $^{2S+1}L_J^{(C)}$ can build up the bound state H. The matrix elements can be seen in equations from (9) to (18):

$$PARP(141) = \langle \mathcal{O}^{J/\psi}[^3S_1^{(1)}]\rangle \quad (9)$$

$$PARP(142) = \langle \mathcal{O}^{J/\psi}[^3S_1^{(8)}]\rangle \quad (10)$$

$$PARP(143) = \langle \mathcal{O}^{J/\psi}[^1S_0^{(8)}]\rangle \quad (11)$$

$$PARP(144) = \langle \frac{\mathcal{O}^{J/\psi}[^3P_0^{(8)}]}{m_c^2}\rangle \quad (12)$$

$$PARP(145) = \langle \frac{\mathcal{O}^{\chi_{c0}}[^3P_0^{(1)}]}{m_c^2}\rangle \quad (13)$$

$$PARP(146) = \langle \mathcal{O}^{\Upsilon}[^3S_1^{(1)}]\rangle \quad (14)$$

$$PARP(147) = \langle \mathcal{O}^{\Upsilon}[^3S_1^{(8)}]\rangle \quad (15)$$

$$PARP(148) = \langle \mathcal{O}^{\Upsilon}[^1S_0^{(8)}]\rangle \quad (16)$$

$$PARP(149) = \langle \frac{\mathcal{O}^{\Upsilon}[^3P_0^{(8)}]}{m_b^2}\rangle \quad (17)$$

$$PARP(150) = \langle \frac{\mathcal{O}^{\chi_{b0}}[^3P_0^{(1)}]}{m_b^2}\rangle \quad (18)$$

The new S-wave processes for $c\overline{c}$ can be seen in Tab. 1. The color singlet contribution ISUB = 421 is completely equivalent to the old definition of the same process, labelled with ISUB=86, apart from the fact that the CSM factors out the wave-function $|R(0)|^2$ at the origin while NRQCD parametrizes the non-perturbative part with NRQCD matrix elements, as seen before. In the χ_c sector, while we had only the gluon-gluon fusion mode in the previous version of PYTHIA (shifted from ISUB = 87-89 to ISUB = 431-433 with rearranged constants as before), now new production mechanisms, gluon-quark and quark-antiquark, are available. A complete reference can be found in Tab. 2. For the bottomonia sector, the new processes implemented are labelled with ISUB = 461 - 470 for S-wave processes and with ISUB = 471 - 479 for χ_b states. A reference for these states is given in Tab. 3 and Tab. 4.

The 10 NRQCD matrix elements are set by default to unphysical values[1] in PYTHIA 6.324, and need proper tuning in order to turn on the respective processes. The actual values have been extracted

[1]Starting from PYTHIA 6.404, the default matrix elements have been set to the values adopted in this note.

ISUB	$g+g \to c\bar{c}[n]+g$	ISUB	$q+g \to q+c\bar{c}[n]$	ISUB	$q+\bar{q} \to g+c\bar{c}[n]$
421	$g+g \to c\bar{c}[^3S_1^{(1)}]+g$				
422	$g+g \to c\bar{c}[^3S_1^{(8)}]+g$	425	$q+g \to q+c\bar{c}[^3S_1^{(8)}]$	428	$q+\bar{q} \to g+c\bar{c}[^3S_1^{(8)}]$
423	$g+g \to c\bar{c}[^1S_0^{(8)}]+g$	426	$q+g \to q+c\bar{c}[^1S_0^{(8)}]$	429	$q+\bar{q} \to g+c\bar{c}[^1S_0^{(8)}]$
424	$g+g \to c\bar{c}[^3P_J^{(8)}]+g$	427	$q+g \to q+c\bar{c}[^3P_J^{(8)}]$	430	$q+\bar{q} \to g+c\bar{c}[^3P_J^{(8)}]$

Table 1 S-wave contributions for $c\bar{c}$ pairs.

ISUB	$g+g \to c\bar{c}[n]+g$	ISUB	$q+g \to q+c\bar{c}[n]$	ISUB	$q+\bar{q} \to g+c\bar{c}[n]$
431	$g+g \to c\bar{c}[^3P_0^{(1)}]+g$	434	$q+g \to q+c\bar{c}[^3P_0^{(1)}]$	437	$q+\bar{q} \to g+c\bar{c}[^3P_0^{(1)}]$
432	$g+g \to c\bar{c}[^3P_1^{(1)}]+g$	435	$q+g \to q+c\bar{c}[^3P_1^{(1)}]$	438	$q+\bar{q} \to g+c\bar{c}[^3P_1^{(1)}]$
433	$g+g \to c\bar{c}[^3P_2^{(1)}]+g$	436	$q+g \to q+c\bar{c}[^3P_2^{(1)}]$	439	$q+\bar{q} \to g+c\bar{c}[^3P_2^{(1)}]$

Table 2 P-wave contributions for $c\bar{c}$ pairs.

ISUB	$g+g \to b\bar{b}[n]+g$	ISUB	$q+g \to q+b\bar{b}[n]$	ISUB	$q+\bar{q} \to g+b\bar{b}[n]$
461	$g+g \to b\bar{b}[^3S_1^{(1)}]+g$				
462	$g+g \to b\bar{b}[^3S_1^{(8)}]+g$	465	$q+g \to q+b\bar{b}[^3S_1^{(8)}]$	468	$q+\bar{q} \to g+b\bar{b}[^3S_1^{(8)}]$
463	$g+g \to b\bar{b}[^1S_0^{(8)}]+g$	466	$q+g \to q+b\bar{b}[^1S_0^{(8)}]$	469	$q+\bar{q} \to g+b\bar{b}[^1S_0^{(8)}]$
464	$g+g \to b\bar{b}[^3P_J^{(8)}]+g$	467	$q+g \to q+b\bar{b}[^3P_J^{(8)}]$	470	$q+\bar{q} \to g+b\bar{b}[^3P_J^{(8)}]$

Table 3 S-wave contributions for $b\bar{b}$ pairs.

ISUB	$g+g \to b\bar{b}[n]+g$	ISUB	$q+g \to q+b\bar{b}[n]$	ISUB	$q+\bar{q} \to g+b\bar{b}[n]$
471	$g+g \to b\bar{b}[^3P_0^{(1)}]+g$	474	$q+g \to q+b\bar{b}[^3P_0^{(1)}]$	477	$q+\bar{q} \to g+b\bar{b}[^3P_0^{(1)}]$
472	$g+g \to b\bar{b}[^3P_1^{(1)}]+g$	475	$q+g \to q+b\bar{b}[^3P_1^{(1)}]$	478	$q+\bar{q} \to g+b\bar{b}[^3P_1^{(1)}]$
473	$g+g \to b\bar{b}[^3P_2^{(1)}]+g$	476	$q+g \to q+b\bar{b}[^3P_2^{(1)}]$	479	$q+\bar{q} \to g+b\bar{b}[^3P_2^{(1)}]$

Table 4 P-wave contributions for $b\bar{b}$ pairs.

PARP(141)	$\langle \mathcal{O}^{J/\psi}[^3S_1^{(1)}] \rangle$	1.16
PARP(142)	$\langle \mathcal{O}^{J/\psi}[^3S_1^{(8)}] \rangle$	0.0119
PARP(143)	$\langle \mathcal{O}^{J/\psi}[^1S_0^{(8)}] \rangle$	0.01
PARP(144)	$\langle \frac{\mathcal{O}^{J/\psi}[^3P_0^{(8)}]}{m_c^2} \rangle$	0.01
PARP(145)	$\langle \frac{\mathcal{O}^{\chi_{c0}}[^3P_0^{(1)}]}{m_c^2} \rangle$	0.05
PARP(146)	$\langle \mathcal{O}^{\Upsilon}[^3S_1^{(1)}] \rangle$	9.28
PARP(147)	$\langle \mathcal{O}^{\Upsilon}[^3S_1^{(8)}] \rangle$	0.15
PARP(148)	$\langle \mathcal{O}^{\Upsilon}[^1S_0^{(8)}] \rangle$	0.02
PARP(149)	$\langle \frac{\mathcal{O}^{\Upsilon}[^3P_0^{(8)}]}{m_b^2} \rangle$	0.02
PARP(150)	$\langle \frac{\mathcal{O}^{\chi_{b0}}[^3P_0^{(1)}]}{m_b^2} \rangle$	0.085

Table 5 Matrix elements values as extracted from [20].

from the Yellow Book publication [20]. The CSM matrix elements are calculated by the Buchmuller-Tye (Eichten-Quigg) potential model [21]. The chosen values for quark masses are $m_c = 1.5\ GeV/c^2$ and $m_b = 4.88\ GeV/c^2$. All the matrix element values are summarized in Tab. 5.

Among the new features, also the Altarelli-Parisi evolution equations for heavy quark pairs have been implemented. The contribution from $Q\overline{Q}[^3S_1^{(8)}]$ partly come from the fragmentation of a gluon. Since the gluon could have split into 2 gluons before fragmentation, this effect has to be included. Two new switches are used: MSTP(148) to switch ON and OFF the splitting $Q\overline{Q}[^3S_1^{(8)}] \rightarrow Q\overline{Q}[^3S_1^{(8)}] + g$, and MSTP(149) to choose if its ensured that the $Q\overline{Q}$ pair always takes the larger fraction of the four-momentum. This obeys the Altarelli-Parisi evolution for $g \rightarrow g + g$. The final state shower evolution, handled with MSTP(148), is allowed both for $c\overline{c}[^3S_1^{(8)}]$ and $b\overline{b}[^3S_1^{(8)}]$. The switching on of MSTP(148) should be performed in a very carefull way because it may exagerate shower effects. In fact not all the $Q\overline{Q}[^3S_1^{(8)}]$ pairs come from the fragmentation component where radiation is expected. Since the fragmentation contribution of $Q\overline{Q}[^3S_1^{(8)}]$ to production processes is the most relevant one, the higher the transverse momentum of the $Q\overline{Q}$ pair is, the more advisable it is to switch on this Altarelli-Parisi evolution. If the $Q\overline{Q}[^3S_1^{(8)}]$ states are allowed to radiate, the parameter MSTP(149) determines the kinematics of the $Q\overline{Q}[^3S_1^{(8)}] \rightarrow Q\overline{Q}[^3S_1^{(8)}] + g$ branching. In our studies we have set both MSTP(148) and MSTP(149) to 1, i.e. the radiation was switched ON and the showering had the same splitting description as for the $g \rightarrow gg$ branching[2].

Another recently introduced feature is the polarization. In fact the hard partonic amplitude squared splitted into its density matrix elements $\rho_{\lambda_1,\lambda_2}$ has been implemented. The variable MSTP(195) allows to switch from unpolarized generation of quarkonia, MSTP(195)=0, to the generation of distinct helicity states (or distinct components of the density matrix), MSTP(195)=1. The expressions for the density matrix elements are taken from [18] and [19] for J/ψ and χ_c production respectively.

Different polarization frames can be selected through the MSTP(196) parameter:

- MSTP(196) = 1 corresponds to the recoil frame;
- MSTP(196) = 2 to the Gottfried-Jackson frame;
- MSTP(196) = 3 to the target frame;
- MSTP(196) = 4 to the Collins-Soper frame.

The selection of the different helicity states or density matrix is done through MSTP(147) (with MSTP(145)=1) according to its different six values. For more details refer to the PYTHIA manual.

[2]Note that the behavior of PYTHIA by using these switches is going to change in release 6.412, since it was found that currently the MSTP(148)=0 option does not fully switch OFF radiation but only provides it at a reduced rate. Please refer to the PYTHIA documentation updates for the details.

5 Simulation settings

For the tuning and testing of these new processes we tried to reproduce the experimental results of proton-antiproton collisions for the J/ψ production at Tevatron Run II (1960 GeV/c^2 center of mass energy) and for the Υ production at Tevatron Run I (1800 GeV/c^2 center of mass energy). The processes that have been turned on in this kind of simulation are all the previously mentioned ones: for charmonium S-wave the processes turned on are those numbered from 421 to 430, for charmonium P-wave all the processes from 431 to 439; for $b\overline{b}$ production, the S-wave processes are those numbered from 461 to 470 while for P-wave those from 471 to 479. In the simulation we have taken into account only the J/ψ directly produced or coming from χ_c decays (excluding all decays from B mesons). For the Υ we have considered only the $\Upsilon(1S)$ production, once again both directly produced and from χ_b. The rapidity region has been chosen according to CDF real data: $-0.6 < y < 0.6$ for J/ψ production and $-0.4 < y < 0.4$ for $\Upsilon(1S)$ production. The *PDF* set used is CTEQ6L.

5.1 Low p_T divergencies in PYTHIA

All the cross-sections of the CSM and COM processes here considered are divergent at leading-order for p_T tending to zero. In fact QCD perturbation theory breaks down at low p_T values because confinement is not taken into account. From a phenomenological point of view, a way out is to allow for a screening related to the inverse color correlation length in protons. On a practical point of view this is implemented in PYTHIA through the introduction of a minimum p_T cut-off, that can be treated in two different ways: an abrupt cut-off, or an appropriately smoothed one defined by a reweighting of the cross-section by a factor [22]:

$$W(p_T, p_{T_0}) = \frac{p_T^4}{(p_{T_0}^2 + p_T^2)} \tag{19}$$

together with a damping of the strong coupling:

$$\alpha_s(p_T^2) \rightarrow \alpha_s(p_{T_0}^2 + p_T^2). \tag{20}$$

In this last approach the cross section gets damped at small p_T according to the value of the phenomenological parameter p_{T_0}: for $p_T >> p_{T_0}$ the standard QCD perturbation theory is recovered, while at small p_T the cross section gets strongly damped. We will investigate first the so called "abrupt cut" approach, tunable in PYTHIA with the parameter CKIN(5).

5.1.1 *First approach: J/ψ production with CSM+COM at various min. p_T cuts*

We generated 10 millions of J/ψ events with the simulation settings described before, turning on first only the CSM processes, and then other 10 millions of events turning on only the COM processes. The p_T cut initially chosen was at 1 GeV/c, setting the value of the abrupt cut by the CKIN(5) parameter. These CKIN parameters define kinematic cuts that can be set before the PYINIT call, and that affect the region of phase space within which events are generated. In the present case CKIN(5) defines a lower cut-off on $\widehat{p}_\perp$ for hard $2 \rightarrow 2$ processes that are singular in the limit $\widehat{p}_\perp \rightarrow 0$, with the transverse momentum $\widehat{p}_\perp$ defined in the rest frame of the hard interaction.

The results for the simulation of the separate CSM and COM components and for the sum of the two can be seen in Fig. 2. This simulation has been compared to the differential cross-section measured by CDF [23]. This experimental sample was particulary suitable for this kind of analysis, extending its values to the lowest p_T region.

As it clearly appears, the minimum p_T cut at 1 GeV/c is completely unsatisfactory in the description of real data. The PYTHIA cross-section is an order of magnitude bigger than experimental data, failing mostly at low p_T values.

The comparisons with real data have been repeated with different kinematic cuts, at 2.0 GeV/c and 2.5 GeV/c, as shown in Fig. 3. For both cuts the superpositions with real data are again unsatisfactory, particularly in the low p_T region. For the 2.0 GeV/c cut, the MC shape still exceeds the data, while for 2.5 GeV/c the peak is lowered and shifted at higher energies, and we are still unable to reproduce the real data behavior, that starts to exceed the MC shape in the very low p_T region.

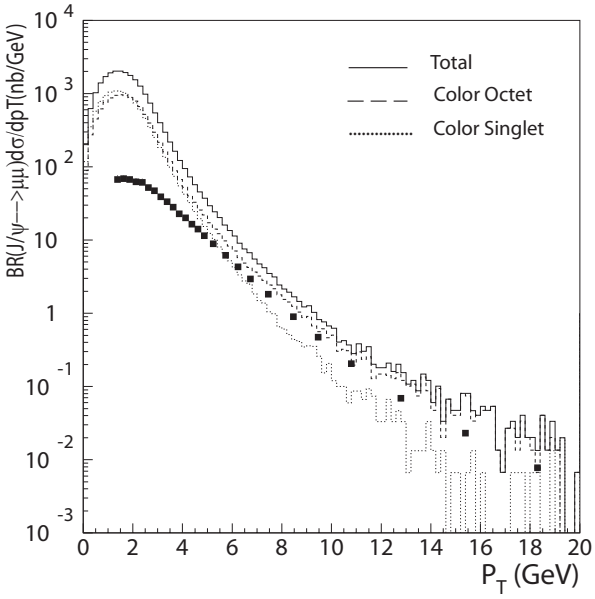

Figure 2 Superposition of CDF data [23] with MC simulation, using the CKIN(5) "abrupt cut" at 1 GeV/c. On the x-axis the p_T of J/ψ is shown, while on the y-axis the differential J/ψ cross-section times branching ratio to $\mu\mu$. The dotted histogram represents the CSM contribution, the dashed one illustrates the COM contribution and the solid one represents the total differential cross-section.

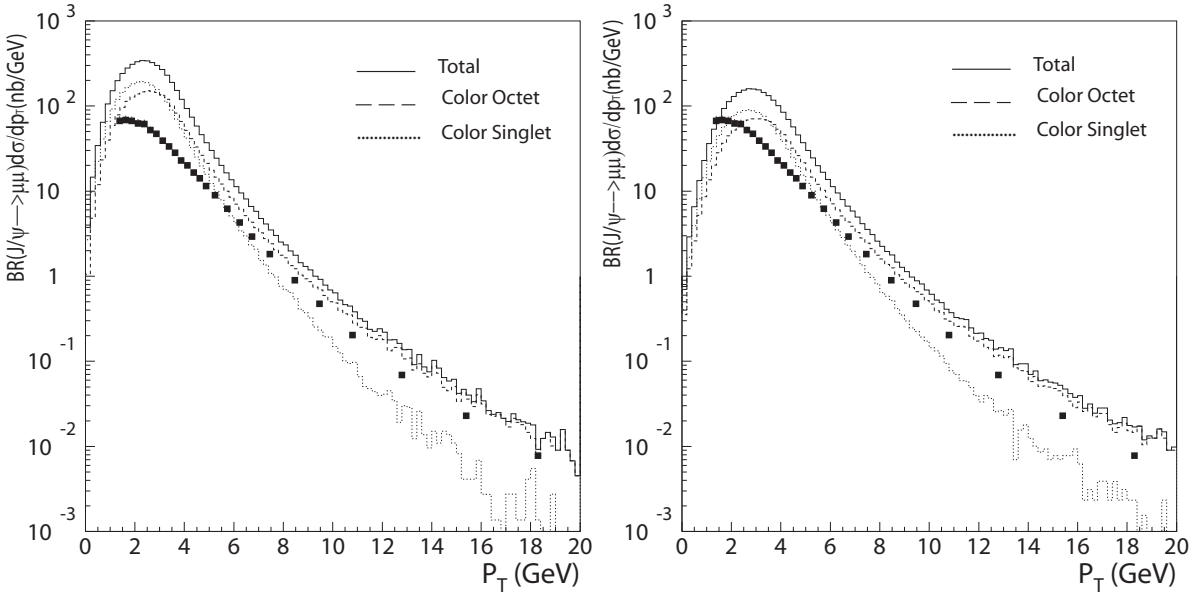

Figure 3 Superposition of CDF [23] data with MC simulation, using the CKIN(5) "abrupt cut" at 2 GeV/c (left plot) and 2.5 GeV/c (right plot).

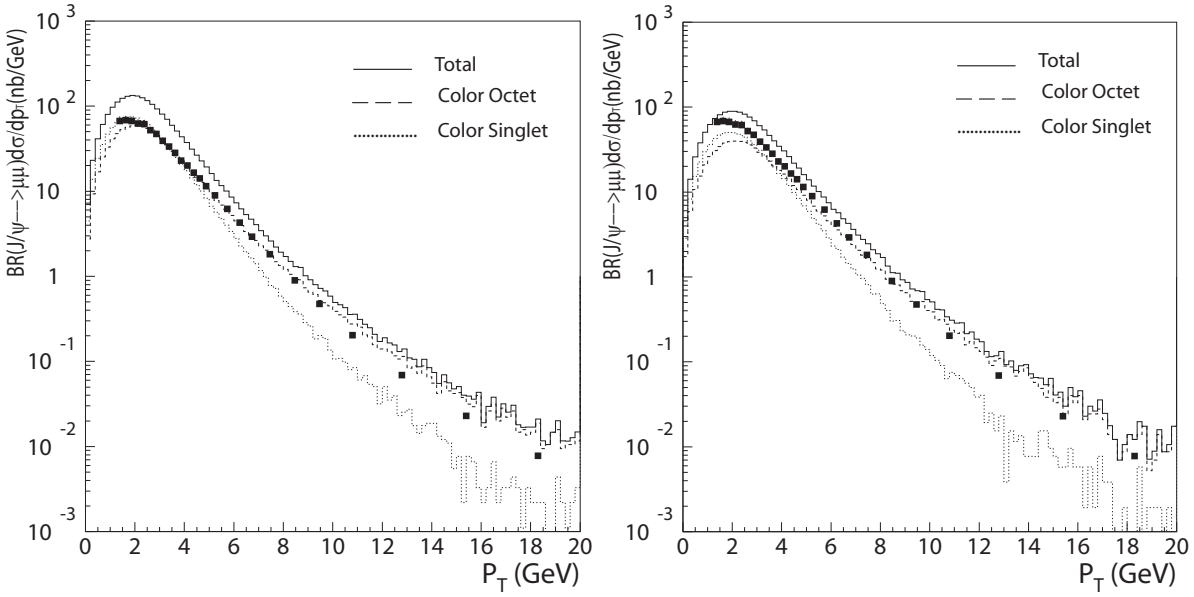

Figure 4 Superposition of CDF [23] data with MC simulation at 2.5 GeV/c (on the left) and 2.85 GeV/c (right figure) values of p_{T_0}. The overall agreement is much better than before: the MC shape follows the experimental data even in the low p_T region, with a better agreement for a p_{T_0} at 2.85 GeV/c.

5.1.2 Second approach: smoothing the cross-section by reweighting

A different approach involves the use of the PYTHIA routine **PYEVWT** that, turned on by setting MSTP(142) = 2, allows to reweight the event cross-section by process type and kinematics of the hard scattering. The parameter MSTP(142) set to 2 indicates that the real cross-section has to be modified by a multiplicative factor defined in PYEVWT. The generated events therefore come with unit weight, as usual, and are then accepted or rejected according to such a weight factor.

In this approach, unlike the abrupt cut-off governed by CKIN(5) that cuts as a step function, we use the PYEVWT function to reweight the cross-section, using a weight defined by Eq. (19). As before, 10 millions of events have been generated, separately for CSM and COM. The comparison with data has been performed with the choice of two different values of p_{T_0}: p_{T_0}=2.5 GeV/c and 2.85 GeV/c. The results can be seen in Fig. 4. The agreement is now surely improved: for the 2.5 GeV/c the MC simulation is still exceeding the data, but the simulation follows the shape of real data. For 2.85 GeV/c the agreement is much better, with the MC shape following accordingly the differential cross-section real data, even at low p_T values.

However some issues are still present:

- The CSM cross-section at high p_T exceeds what we would have expected, and this explains partially a slight excess of the sum of the two contributions;
- the optimal p_{T_0} value is slightly on the large side; in fact a value around 2-2.5 GeV/c, in strict analogy to the value used in the multiple parton interaction scheme in PYTHIA, which adopts the same concept and mechanism for damping the divergent cross-sections at low p_T, would be preferrable, in order to have a "universal" picture. This fact could be also partly explained by an excess of CSM contributions at low p_T.

5.2 Υ production

Some studies have been performed also for $\Upsilon(1S)$ production. As said before, only direct production and decays from χ_b have been considered. The rapidity region considered for this production is $-0.4 < y < 0.4$, to match the available experimental data. Two millions of events have been generated for the CSM production, where we have turned on processes ISUB = 461 and ISUB = 471 to 479. In

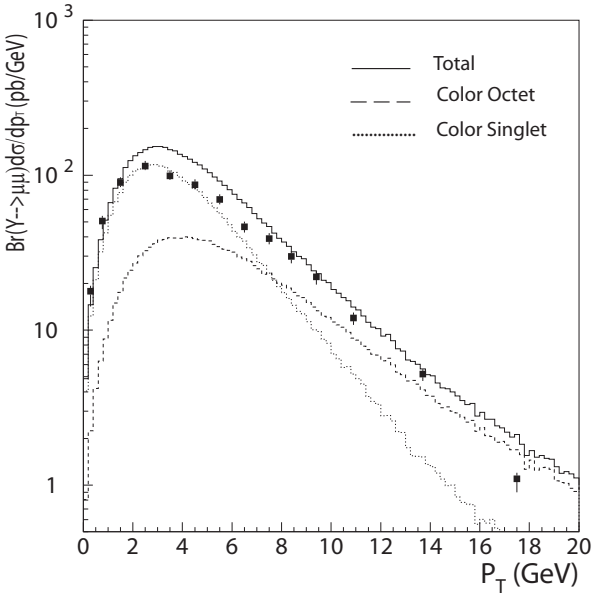

Figure 5 Superposition of $\Upsilon(1S)$ cross-section measured by CDF [24] with MC prediction. The p_{T_0} value is set as before to 2.85 GeV/c. The overall agreement is fairly good.

the same way, a COM production with two millions of events produced has been run, turning on all the processes from ISUB = 462 to 470. The sum of the two productions has then been compared with a CDF Run I data [24]. As before the *PDF* chosen for this analysis is CTEQ6L. Once again the cross section value has been re-weighted according to the re-weighting approach presented before. The p_{T_0} value used in the simulation is the optimal one determined for the J/ψ production, 2.85 GeV/c. The comparison of the experimental differential cross-section with the MC prediction can be seen in Fig. 5. The general agreement between data and MC appears fairly good, particularly in the low p_T region between 0 GeV/c and 3 GeV/c. In the central region between 4 GeV/c and 7 GeV/c the MC differential cross-section slightly overestimates the data. The agreement at higher p_T is good.

6 Perspectives at LHC

In order to produce a coherent picture at the LHC energy, we need to have a correct extrapolation of the p_{T_0} value, previously determined at lower energies. In fact p_{T_0} in principle should not be energy independent. In strict analogy to the PYTHIA model of multiple parton interactions that is applied by default for all the QCD $2 \to 2$ processes [25], p_{T_0} is assumed to exhibit a dependence on energy of the form:

$$p_{T0} \to p_{T0}(\frac{\sqrt{s}}{E_0})^{\vartheta}. \tag{21}$$

Different studies have been carried out: a reasonable value of ϑ, according to the tunings of the PYTHIA multiple parton interaction model, is expected to be around 0.16 [26]. Here we have considered different scenarios, starting from a ϑ value equal to zero, implying no energy dependence of p_{T_0}, ranging to 0.2. The cross-sections have been calculated according to the different rapidity regions of LHC experiments:

- $-2.5 < y < 2.5$ for the Atlas/CMS rapidity region;
- $1.8 < y < 4.9$ for the LHCb region.

The complete view of the evaluated cross-sections, for the different conditions, can be seen in Tab. 6. The total cross-section times $BR_{\mu\mu}$ is ranging from $5.5\mu b$ to $15\mu b$. The values of the cross-sections in the different acceptance regions and integrated over the full solid angle are also shown in Fig. 6.

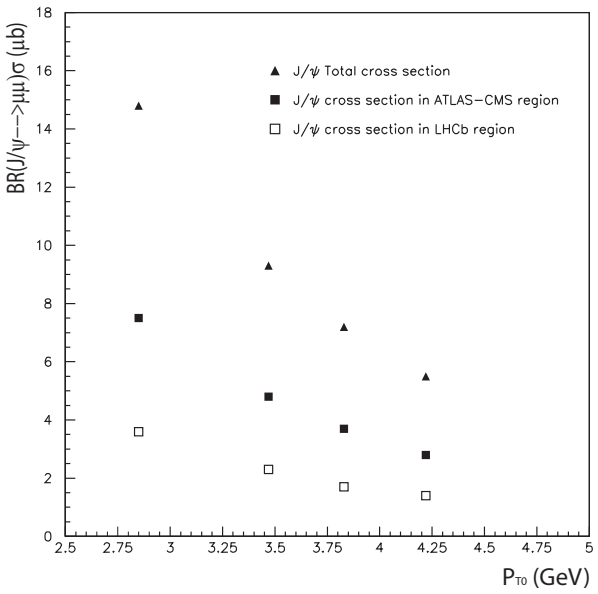

Figure 6 Total J/ψ cross-section times the branching ratio to $\mu\mu$ as a function of p_{T_0}. The different symbols refer to the cross-sections calculated in different LHC acceptance regions, and to the total J/ψ cross-section integrated over the full solid angle.

ϑ	p_{T0}(GeV)	$BR_{\mu\mu}\sigma_{Tot}[\mu b]$	$BR_{\mu\mu}\sigma_{Atlas,CMS}[\mu b]$	$BR_{\mu\mu}\sigma_{LHCb}[\mu b]$
0	2.85	14.8	7.5	3.6
0.1	3.47	9.3	4.8	2.3
0.15	3.83	7.2	3.7	1.7
0.2	4.22	5.5	2.8	1.4

Table 6 J/ψ cross-section at LHC as a function of the extrapolation of p_{T0} to the LHC energy, using different values of ϑ (see text). For each value of ϑ are indicated: the corresponding value of p_{T0}, the total J/ψ cross-section times the branching ratio to $\mu\mu$, and the total two cross-sections within the Atlas/CMS and LHCb acceptances. We have used $BR_{\mu\mu} = 0.0588 \pm 0.0010$.

Finally, as an example, we have produced differential spectra at the LHC energy, both for the Atlas/CMS region and the LHCb one, using a ϑ value of 0.1, corresponding to a p_{T_0} value of about 3.5 GeV/c. They can be seen in Fig. 7.

7 Conclusions

The inclusion of COM contributions in PYTHIA, using different min. p_T cut-offs for regularizing the divergent cross-section at $p_T \to 0$, gives unsatisfactory results if an abrupt p_T cut-off is used, when comparing simulations of J/ψ prompt production with CDF data. Instead, more promising results have been achieved with event-by-event reweighting adopting the same scheme used in the PYTHIA multiple parton interaction model, both for J/ψ and Υ production at the Tevatron. However, the contribution from CSM seems a bit excessive with respect to what we expected, and needs to be better understood. We have performed an extrapolation of the re-weighting parameter p_{T_0} to the LHC energy in different scenarios of energy dependence. The total cross-section for prompt J/ψ (times $BR_{\mu\mu}$) production at the LHC is predicted in the range 5.5-15 μb.

Acknowledgments

The authors wish to warmly acknowledge T. Sjostrand and P. Bartalini for their interest, encouragement, suggestions, useful discussions and technical support. Many thanks also to our LHCb colleague L. Camilleri for his very careful review of the manuscript.

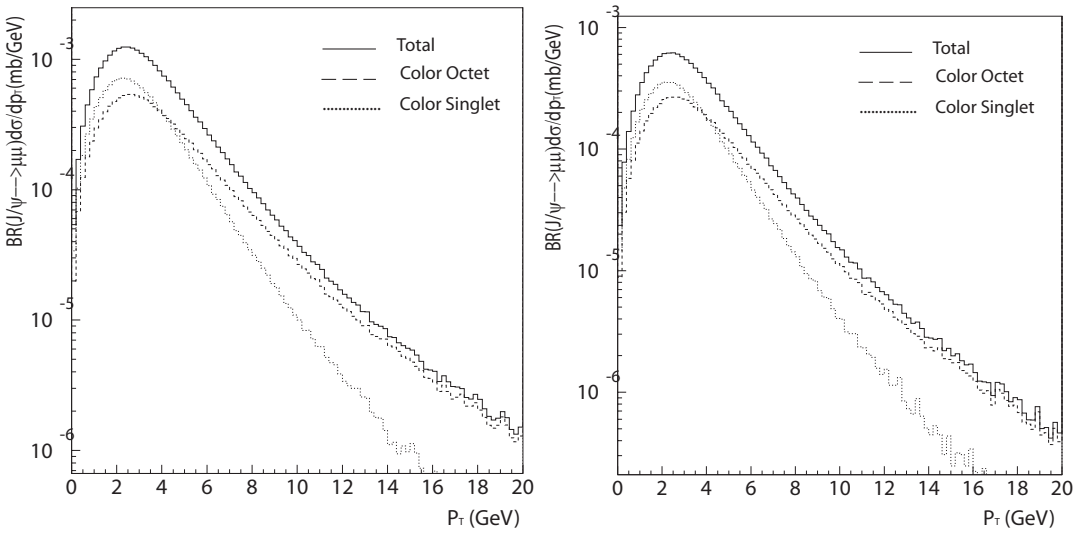

Figure 7 Differential cross-sections at LHC for the Atlas/CMS region ($-2.5 < y < 2.5$), on the left side, and for the LHCb one ($1.8 < y < 4.9$), on the right. The chosen value for the ϑ parameter is 0.1.

References

[1] Sjostrand T., Mrenna S. and Skands P., JHEP **0605** (2006) 026 [arXiv:hep-ph/0603175].

[2] Schuler G. A., 'Quarkonium production and decays', CERN report CERN-TH-7170-94, [hep-ph/9403387], and references therein.

[3] Gavai R. et al., Int. J. Mod. Phys., **A10** (1995), 3043, hep-ph/9502270.

[4] Bodwin G.T., Braaten E. and Lepage G.P., Phys. Rev., **D51**, 1125 (1995) [hep-ph/9407339], erratum *ibid.* **D55**, 5853 (E) (1997).

[5] Caswell W.E., Lepage G. P., Phys. Lett., **167**, 437 (1986).

[6] Lepage G.P., Magnea L., Nakhleh C., Magnea U. and Hornbostel K., Phys. Rev., **D46**, 4052 (1992).

[7] Braaten E., Yuan T.C., Phys Rev. Lett., **71**, 1673 (1993).

[8] Cacciari M., Greco M., Phys. Rev. Lett., **73**, 1586 (1994).

[9] Braaten E., Donchescki M.A., Fleming S., Mangano M.L., Phys Lett., **B333**, 548 (1994).

[10] Cho P., Leibovich A.K., Phys. Rev. **D53**, 150 and 6203 (1996).

[11] Beneke M., Rothstein I.Z., Phys. Rev., **D54**, 2005 (1996).

[12] Bodwin G.T., Braaten E. and Lepage G.P., Phys. Rev., **D46**, 1914 (1992), [hep-lat/9205006].

[13] Braaten E., Chen Y.-Q., Phys Rev **D54**, 3216 (1996).

[14] Cacciari M., Krämer M., Phys. Rev. Lett., **76**, 4128 (1996).

[15] Bodwin G.T., Braaten E., Yian T.C. Lepage G.P., Phys. Rev. **D46**, R3703 (1992).

[16] Beneke M., Krämer M., Phys. Rev., **D55**, 5269 (1997).

[17] Stefan Wolf, private communication.

[18] Beneke M., Krämer M.,Vänttinen M., Phys. Rev.**D57** (1998) 4258 [hep-ph/9709376].

[19] Kniehl B.A., Lee J., Phys Rev., **D62** (2000) 114027 [hep-ph/0007292].

[20] Nason P. *et al.*, arXiv:hep-ph/0003142.

[21] Eichten E., Quigg C., Phys.Rev. **D52**:1726-1728,1995, hep-ph/9503356.

[22] Sjostrand T. et al., Phys. Rev. **D36**:2019, 1987.

[23] CDF Collaboration, Phys. Rev. **D71**: 032001, 2005.

[24] CDF Collaboration, Phys Rev. Lett. **88**, 161802 (2002).

[25] Sjostrand T. and Skands P., JHEP **0403**, 053 (2004) [arXiv:hep-ph/0402078].

[26] Bartalini. P *et al.*, LHCb public note 99-028.